

Slip velocity of lattice Boltzmann simulation using bounce-back boundary scheme

Jianping Meng,^{*} Xiao-Jun Gu,[†] and David R Emerson[‡]

Scientific Computing Department, STFC Daresbury laboratory,

Warrington WA4 4AD, United Kingdom

(Dated: August 11, 2015)

Abstract

In this work we investigate the issue of non-physical slip at wall of lattice Boltzmann simulations with the bounce-back boundary scheme. By comparing the analytical solution of two lattice models with four and nine discrete velocities for the force-driven Poiseuille flow, we are able to reveal the exact mechanism causing the issue. In fact, no boundary condition is defined by the bounce-back scheme for the the discrete velocities parallel to wall. Other factors, such as initial conditions and inlet and outlet boundary conditions, can play the role and induce the non-physical slip velocity. Therefore, the issue is not related to the single-relaxation-time scheme. Naturally the key for resolving it is to specify the definition for these velocities. Through a lid-driven cavity flow, we show that the solution can be as easy as no extra effort required for simple geometries, although further study is necessary for complex geometries.

^{*} To whom correspondence should be addressed: jianping.meng@stfc.ac.uk

[†] xiaojun.gu@stfc.ac.uk

[‡] david.emerson@stfc.ac.uk

I. INTRODUCTION

The lattice Boltzmann method (LBM) has been developed as a mesoscopic computational fluid dynamics (CFD) tool for the Navier-Stokes (NS) level problems and beyond [1–3]. Due to its origin from the lattice gas automata (LGA) [4], it keeps the flexibility of a particle method to a great extent. On the other hand, the stochastic noise is eliminated in LBM by using the distribution function. Importantly, this links the LBM into the discrete velocity method of the Boltzmann-BGK (Bhatnagar-Gross-Krook) equation [5–8]. From such a point of view, we actually solve a system of partial differential equations with linear advection terms. This opens the door of introducing more sophisticated scheme leading to such as finite difference LBM or finite volume LBM (e.g., [9] and [10]).

It is the simplicity which brings the popularity of LBM. The algorithm is easy to understand for application purpose. Since an explicit scheme is employed, the programming and parallelism is straightforward. The second order accuracy in both space and time is achieved at the expense of a first order scheme, which is fairly enough for most purposes. The boundary treatment, even for complex geometry, can be incredibly simple due to the so-called bounce-back (BB) scheme which only requires the particles to reverse their velocity on the wall/obstacle [11, 12].

However, there are non-physical slip velocities occurring at wall in simulations using the BB scheme. This was firstly discovered for two LGA models [11] and then was analysed for the nine-discrete-velocity (D2Q9) LBM in [12]. By using a simple force-driven Poiseuille flow, it was shown that the non-physical slip can be generated on the wall with the BB family scheme [12]. Since the slip velocity was found to be related to the mesh size, it was then deemed as a numerical artificial effect. Later, this issue has been considered as an inherent deficiency of the single-relaxation-time (SRT) scheme since it may be resolved by using extra free parameters in two-relaxation-time (TRT) or multi-relaxation time (MRT) schemes (see e.g. [13]). Indeed, it is believed that the SRT plus BB combination cannot avoid this issue [14].

However, due to its simplicity, the SRT plus BB combination is more favourable for application purpose. Therefore, it is of interest to investigate how the slip velocity is induced and therefore gain useful information on how to fix it. For this purpose, we will first analysis a lattice model with four discrete velocities (D2Q4) for the force-driven Poiseuille flow following

the method presented in [12]. With this lattice model, we will see that the SRT plus BB combination does not necessarily induce non-physical slip velocity and it is possible to correctly implement the non-slip wall. Then we will compare this model with the D2Q9 model to find the exact mechanism inducing the slip velocity. With these findings, we devise a guidance on how to fix the non-physical slip velocity. Finally, we will examine this guidance and thereby the discussions on the mechanism by simulating the lid-driven cavity flow with the D2Q9 lattice.

II. LATTICE BOLTZMANN SCHEME AND LATTICES

The LBM can be considered as an approximation to the Boltzmann-BGK equation [5–8]. After the discretisation in the particle velocity space, the governing equation becomes

$$\frac{\partial f_\alpha}{\partial t} + \mathbf{C}_\alpha \cdot \nabla f_\alpha = -\frac{1}{\tau}(f_\alpha - f_\alpha^{eq}) + F_\alpha, \quad (1)$$

which represents the evolution of the distribution function $f_\alpha(\mathbf{r}, t)$ for the α th discrete velocity \mathbf{C}_α at position $\mathbf{r} = (x, y, z)$ and time t . The effect of external body force is described by F_α . The particle interaction is modelled by a relaxation term towards the discrete equilibrium distribution function $f_\alpha^{eq}(\mathbf{r}, t)$. In order to simulate incompressible and isothermal flows, it is common to use an equilibrium function with second order velocity terms, i.e.,

$$f_\alpha^{eq} = w_\alpha \rho \left[1 + \frac{\mathbf{U} \cdot \mathbf{C}_\alpha}{RT_0} + \frac{1}{2} \frac{(\mathbf{U} \cdot \mathbf{C}_\alpha)^2}{(RT_0)^2} - \frac{\mathbf{U} \cdot \mathbf{U}}{2RT_0} \right], \quad (2)$$

which is determined by the density, ρ , the fluid velocity, \mathbf{U} , and the reference temperature, T_0 . For gas flows, the constant, R , can be conveniently understood as the gas constant. If a liquid fluid is involved, it, together with T_0 , can be considered as a reference quantity. For convenience, the sound speed c_s is often considered equal to $\sqrt{RT_0}$, although there is a constant factor of difference. The weight factor is denoted by w_α for the discrete velocity \mathbf{C}_α . The term F_α can be obtained by using various method [8, 15]. Here, the first order expansion is sufficient for our purpose, which can be written as [8].

$$F_\alpha = \rho w_\alpha \frac{\mathbf{G} \cdot \mathbf{C}_\alpha}{RT_0}. \quad (3)$$

where the actual induced acceleration is denoted by \mathbf{G} . The relaxation time, τ , is related to the fluid viscosity, μ , and the pressure, p , via the Chapman-Enskog expansion, i.e.,

$\mu = p\tau$. Hence, for isothermal and incompressible flows, the Reynolds number becomes $Re = \rho_0 U_0 L / \mu = U_0 L / (\tau RT_0)$, where we use a subscript 0 to denote the reference value and L the characteristic length of the system. It is worth noting here that the Knudsen number can be defined as $\mu_0 \sqrt{RT_0} / (p_0 L)$. So, the relaxation time τ is also related to Knudsen number by the viscosity $Kn = \tau \sqrt{RT_0} / L$, where $p_0 = \rho_0 RT_0$ is applied. In this sense, we have $Kn \times Re = U_0 / \sqrt{RT_0} = Ma$. To get the density and velocity, we only need summation operations, i.e.,

$$\rho = \sum_{\alpha} f_{\alpha}, \text{ and, } \rho \mathbf{U} = \sum_{\alpha} f_{\alpha} \mathbf{C}_{\alpha}.$$

To numerically solve Eq. (1), a smart trapezoidal scheme can be used to achieve the particle-jump like simulation [16], which can be written as

$$\tilde{f}_{\alpha}(\mathbf{r} + \mathbf{C}_{\alpha} dt, t + dt) - \tilde{f}_{\alpha}(\mathbf{r}, t) = -\frac{dt}{\tau + 0.5dt} \left[\tilde{f}_{\alpha}(\mathbf{r}, t) - f_{\alpha}^{eq}(\mathbf{r}, t) \right] + \frac{\tau F_{\alpha} dt}{\tau + 0.5dt}, \quad (4)$$

where

$$\tilde{f}_{\alpha} = f_{\alpha} + \frac{dt}{2\tau} (f_{\alpha} - f_{\alpha}^{eq}) - \frac{dt}{2} F_{\alpha}. \quad (5)$$

By using \tilde{f}_{α} this scheme is ready for implementing the stream-collision algorithm. At the same time, the macroscopic quantities become

$$\rho = \sum_{\alpha} \tilde{f}_{\alpha}, \text{ and, } \rho \mathbf{U} = \sum_{\alpha} \mathbf{C}_{\alpha} \tilde{f}_{\alpha} + \frac{\rho \mathbf{G} dt}{2}. \quad (6)$$

For two dimensional flows, the D2Q9 lattice is commonly used where the nine discrete velocities ($\alpha = 1..9$) are

$$\mathbf{C}_{\alpha,x} = \sqrt{3RT_0} [0, 1, 0, -1, 0, 1, -1, -1, 1], \quad (7)$$

$$\mathbf{C}_{\alpha,y} = \sqrt{3RT_0} [0, 0, 1, 0, -1, 1, 1, -1, -1], \quad (8)$$

and the corresponding weights are

$$w_{\alpha} = \left[\frac{4}{9}, \frac{1}{9}, \frac{1}{9}, \frac{1}{9}, \frac{1}{9}, \frac{1}{36}, \frac{1}{36}, \frac{1}{36}, \frac{1}{36} \right]. \quad (9)$$

As discussed above, the stream-collision algorithm is ready to be implemented now. The only trick is to tie the space and time step together as $d\mathbf{r} = \mathbf{C}_{\alpha} dt$. For instance, assuming the system length is L , we may set the spatial step $dx = L/N$ and then $dt = L / (N\sqrt{3RT_0})$

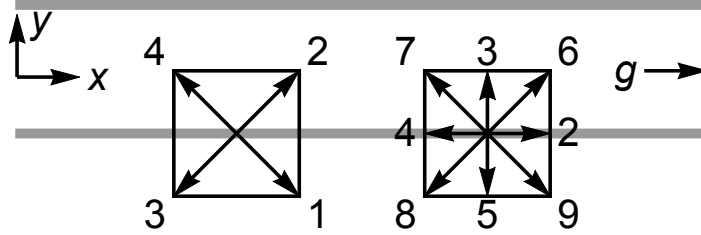


Figure 1. Illustration of the D2Q4 and D2Q9 lattice at the bottom wall for a force-driven Poiseuille flow. The discrete velocity $\mathbf{C}_1 = (0, 0)$ of the D2Q9 lattice is not shown.

where N is the cell number. This insures the “particles” are jumping on a uniform grid system. In simulations, it is common practice to use a non-dimensional system in which the space and time step are considered as reference value. Apparently, this will make no difference on results. However, confusion may be caused in this way. We shall return to this point below. Alternatively, we may also transform Eq. (1) to its non-dimensional form first by using the reference values presented in [17] and then apply the scheme Eq. (4). Again, this non-dimensional transformation will not alter the final simulation results but the relations with dimensional quantities are more clear, at least for gas dynamics.

To study the effect of the BB scheme on the solid boundary, we will first use a D2Q4 model [8] where the four discrete velocities are

$$C_{\alpha,x} = \sqrt{RT_0}[1, 1, -1, -1], \quad (10)$$

$$C_{\alpha,y} = \sqrt{RT_0}[-1, 1, -1, 1], \quad (11)$$

and the weights are

$$w_\alpha = \left[\frac{1}{4}, \frac{1}{4}, \frac{1}{4}, \frac{1}{4}\right]. \quad (12)$$

Both the D2Q9 and D2Q4 models are illustrated in Fig. 1. It is worth noting that in the D2Q4 model there is no discrete velocity parallel to the wall for the force-driven Poiseuille flow with regular shaped channel (i.e., the wall is either horizontal or vertical), which will make a dramatical difference from the D2Q9 model for the force-driven Poiseuille flow.

III. SLIP VELOCITY AND BOUNCE-BACK SCHEME

A. Solution of D2Q4 model for force-driven Poiseuille flow

In the following, we will use the method presented in [12] to solve the D2Q4 model for the force-driven Poiseuille flow. For convenience, we introduce some new notations $\mathbf{G}/\sqrt{RT_0} = (g_x, g_y)$, $\mathbf{U}/\sqrt{RT_0} = (u, v)$ and $\mathbf{C}/\sqrt{RT_0} = \mathbf{c} = (c_x, c_y)$. This is just for the simplicity of formulations and should not be understood as a non-dimensional transformation in this work. Instead, we stick to the dimensional system presented in Eqs. (1) and (4). Moreover, for convenience, we use letter A to denotes the coefficient $dt/(\tau + 0.5dt)$ of the relaxation term and B for the coefficient $\tau dt/(\tau + 0.5dt)$ of the force term. Without influencing the discussion, we set g_y and v to be zero. Therefore, for the D2Q4 lattice, the evolutionary rules for the j th bulk node are

$$\tilde{f}_{j,1} = (1 - A)\tilde{f}_{j+1,1} + \frac{1}{4}A\rho u_{j+1} + \frac{A\rho}{4} + \frac{Bg_x\rho}{4}, \quad (13a)$$

$$\tilde{f}_{j,2} = (1 - A)\tilde{f}_{j-1,2} + \frac{1}{4}A\rho u_{j-1} + \frac{A\rho}{4} + \frac{Bg_x\rho}{4}, \quad (13b)$$

$$\tilde{f}_{j,3} = (1 - A)\tilde{f}_{j+1,3} - \frac{1}{4}A\rho u_{j+1} + \frac{A\rho}{4} - \frac{Bg_x\rho}{4}, \quad (13c)$$

$$\tilde{f}_{j,4} = (1 - A)\tilde{f}_{j-1,4} - \frac{1}{4}A\rho u_{j-1} + \frac{A\rho}{4} - \frac{Bg_x\rho}{4}, \quad (13d)$$

while Eq. (6) for the velocity becomes

$$\rho u_j = \tilde{f}_{j,1} + \tilde{f}_{j,2} - \tilde{f}_{j,3} - \tilde{f}_{j,4} + \frac{\rho g_x dt}{2}. \quad (14)$$

To get the macroscopic governing equation, we follow the procedure of [12]. For convenience, we write a few alternative variants of rules Eqs.(13)-(14), i.e.,

$$\tilde{f}_{j-1,1} = (1 - A)\tilde{f}_{j,1} + \frac{1}{4}A\rho u_j + \frac{A\rho}{4} + \frac{Bg_x\rho}{4}, \quad (15a)$$

$$\tilde{f}_{j+1,2} = (1 - A)\tilde{f}_{j,2} + \frac{1}{4}A\rho u_j + \frac{A\rho}{4} + \frac{Bg_x\rho}{4}, \quad (15b)$$

$$\tilde{f}_{j-1,3} = (1 - A)\tilde{f}_{j,3} - \frac{1}{4}A\rho u_j + \frac{A\rho}{4} - \frac{Bg_x\rho}{4}, \quad (15c)$$

$$\tilde{f}_{j+1,4} = (1 - A)\tilde{f}_{j,4} - \frac{1}{4}A\rho u_j + \frac{A\rho}{4} - \frac{Bg_x\rho}{4}, \quad (15d)$$

and

$$\rho u_{j+1} = \tilde{f}_{j+1,1} + \tilde{f}_{j+1,2} - \tilde{f}_{j+1,3} - \tilde{f}_{j+1,4} + \frac{dt g_x \rho}{2}, \quad (16a)$$

$$\rho u_{j-1} = \tilde{f}_{j-1,1} + \tilde{f}_{j-1,2} - \tilde{f}_{j-1,3} - \tilde{f}_{j-1,4} + \frac{dt g_x \rho}{2}. \quad (16b)$$

Applying the rules Eq. (13) into Eq. (14), we have

$$\rho u_j = (1 - A)(\tilde{f}_{j-1,2} - \tilde{f}_{j-1,4} + \tilde{f}_{j+1,1} - \tilde{f}_{j+1,3}) + \frac{1}{2}A\rho u_{j-1} + \frac{1}{2}A\rho u_{j+1} + Bg_x\rho + \frac{dt g_x \rho}{2}. \quad (17)$$

Hence, we need to work out $(1 - A)(\tilde{f}_{j-1,2} - \tilde{f}_{j-1,4} + \tilde{f}_{j+1,1} - \tilde{f}_{j+1,3})$. To do so, the main idea is to use the rules Eqs.(13) and (15) and Eqs. (14) and (16) alternatively. The aim is to relate the unknown distribution functions to the macroscopic quantities. For example, to obtain $\tilde{f}_{j-1,2} - \tilde{f}_{j-1,4}$, we first use (16b) to represent the unknowns with u_{j-1} , $\tilde{f}_{j-1,1}$ and $\tilde{f}_{j-1,3}$, then use rules (15a) and (15c) to transform $\tilde{f}_{j-1,1} - \tilde{f}_{j-1,3}$ into a formula of u_j , $\tilde{f}_{j,1}$ and $\tilde{f}_{j,3}$. Finally, we can apply the rule Eq. (14) to convert all f_j s into a formula of u_j . Following this idea and through a few iterations, we obtain

$$Ag_x\rho(Adt + 2B) + (2 - A)\rho u_{j-1} + 2(A - 2)\rho u_j + (2 - A)\rho u_{j+1} = 0. \quad (18)$$

Considering the meaning of A and B , the equation becomes

$$\rho dt^2 g_x + \rho\tau(u_{j-1} - 2u_j + u_{j+1}) = 0. \quad (19)$$

Further using $dt = dx/\sqrt{RT_0}$, $\mu = p\tau$, and $p_0 = \rho_0 RT_0$, the final form is

$$\frac{\mu(u_{j-1} - 2u_j + u_{j+1})}{dx^2} + \rho g_x = 0, \quad (20)$$

which is exactly the second central difference scheme of the NS equations for this simple force-driven flow. It has a simple solution

$$u_j = \rho g \frac{(L - jdx)jdx}{2\mu} + U_s, \quad j = 0, 1, 2, 3, \dots N. \quad (21)$$

The slip velocity is denoted by U_s , which is produced by the boundary treatment, either physically or non-physically. So, its exact value will depend on the specific boundary condition.

To find U_s , we also follow the procedure of [16]. First, we introduce a notation $U_0 = \sum_{\alpha} c_{\alpha,x} f_{0,\alpha}$ where the incoming distribution functions will be determined by the boundary

condition. In order to find the slip velocity, we actually look at the node $j = 1$. Following the manner of finding the bulk equation, we will be able to obtain the relation of the prescribed boundary speed u_0 , u_1 , u_2 and U_0 . The trick is that the prescribed boundary velocity $(u_0, 0)$ is used when applying Eq. (13) into Eq. (14). However, when using the rule (16b) for $j = 1$, we need to consider the relation $U_0 = \sum_{\alpha} c_{\alpha,x} f_{0,\alpha}$. Through simple calculations, the relation can be written as

$$u_1 = \frac{u_0 + u_2}{2} + \frac{dt^2 g_x}{2\tau} - \frac{(dt - 2\tau)(U_0 - u_0)}{4\tau}. \quad (22)$$

For simplicity, we assume a non-slip boundary with zero speed at wall in the following, i.e., u_0 is set to be zero. Then, substituting the solution (21) into Eq. (22), we can obtain the slip velocity

$$U_s = \frac{2\tau - dt}{2\tau} U_0. \quad (23)$$

For the so called modified BB (MBB) scheme (means that collision and forcing still occur at boundary nodes [12]), the rule at the boundary point is

$$f_{0,4} = f_{0,1} \quad f_{0,2} = f_{0,3}. \quad (24)$$

It can be seen that U_0 must be zero. Hence, for the D2Q4 model, the slip velocity U_s is zero. Although the SRT scheme is used, the MBB scheme leads to a correct non-slip boundary condition. Moreover, if rotating the wall direction from horizontal to vertical, it can be easily seen that slip velocity will also be zero.

For the BB scheme without collision and forcing occurring at boundary nodes, we can not directly apply Eqs. (22) and (23). But it is straightforward to see that U_s will be zero.

As has been shown, the results of D2Q4 model are significantly different from that of the D2Q9 model and D2Q5 model presented in [11, 12]. This helps to clarify the relation between the SRT scheme and non-physical slip velocity. The SRT scheme plus the MBB or BB boundary scheme does not necessarily induces non-physical slip velocity.

B. Mechanism of non-physical slip velocity with D2Q9 model.

Now it is natural to ask why there is non-physical slip velocity in such as the D2Q9 solution. For this purpose, we return to the D2Q9 model following [12]. The rules for the

D2Q9 model are

$$\tilde{f}_{j,1} = \frac{4\rho}{9} - \frac{2\rho u_j^2}{9} \quad (25a)$$

$$\tilde{f}_{j,2} = \frac{\rho u_j^2}{9} + \frac{\rho u_j}{3\sqrt{3}} + \frac{Bg_x\rho}{3\sqrt{3}A} + \frac{\rho}{9} \quad (25b)$$

$$\tilde{f}_{j,3} = -\frac{1}{18}A\rho u_{j-1}^2 + \frac{A\rho}{9} + (1-A)\tilde{f}_{j-1,3} \quad (25c)$$

$$\tilde{f}_{j,4} = \frac{\rho u_j^2}{9} - \frac{\rho u_j}{3\sqrt{3}} - \frac{Bg_x\rho}{3\sqrt{3}A} + \frac{\rho}{9} \quad (25d)$$

$$\tilde{f}_{j,5} = -\frac{1}{18}A\rho u_{j+1}^2 + \frac{A\rho}{9} + (1-A)\tilde{f}_{j+1,5} \quad (25e)$$

$$\tilde{f}_{j,6} = \frac{1}{36}A\rho u_{j-1}^2 + \frac{A\rho u_{j-1}}{12\sqrt{3}} + \frac{A\rho}{36} + \frac{Bg_x\rho}{12\sqrt{3}} + (1-A)\tilde{f}_{j-1,6} \quad (25f)$$

$$\tilde{f}_{j,7} = \frac{1}{36}A\rho u_{j-1}^2 - \frac{A\rho u_{j-1}}{12\sqrt{3}} + \frac{A\rho}{36} - \frac{Bg_x\rho}{12\sqrt{3}} + (1-A)\tilde{f}_{j-1,7} \quad (25g)$$

$$\tilde{f}_{j,8} = \frac{1}{36}A\rho u_{j+1}^2 - \frac{A\rho u_{j+1}}{12\sqrt{3}} + \frac{A\rho}{36} - \frac{Bg_x\rho}{12\sqrt{3}} + (1-A)\tilde{f}_{j+1,8} \quad (25h)$$

$$\tilde{f}_{j,9} = \frac{1}{36}A\rho u_{j+1}^2 + \frac{A\rho u_{j+1}}{12\sqrt{3}} + \frac{A\rho}{36} + \frac{Bg_x\rho}{12\sqrt{3}} + (1-A)\tilde{f}_{j+1,9}. \quad (25i)$$

As discussed before, we will pay particular attention to discrete velocities parallel to the wall. With the horizontal wall, they are the 2nd and 4th velocity as shown in Fig. 1. Looking at Eqs. (25b) and (25d), we remind that they are mainly the consequence of periodic boundary conditions for the inlet and outlet, i.e., there is no gradient in the streamwise direction. In other words, they are not solely related to the SRT scheme and are NOT determined by the BB scheme at all. Similarly, the governing equation for bulk nodes is

$$\frac{\mu(u_{j-1} - 2u_j + u_{j+1})}{dx^2} + 3dt_9^2\rho g_x = 0, \quad (26)$$

where dt_9 means the time step for the D2Q9 model. Assuming the space step is same for both two models, $dt_9 = dt/\sqrt{3}$ where dt is time step for the D2Q4 model. Hence two models yield same governing equation for momentum. For brevity, we only discuss the MBB scheme.

Therefore, u_1 and U_s can be written as

$$u_1 = \frac{u_0 + u_2}{2} + \frac{dt_9^2 g_x}{2\tau} - \frac{3(dt_9 - 2\tau)(U_0 - u_0)}{4\tau} \quad (27)$$

and

$$U_s = \frac{3(2\tau - dt_9)}{2\tau} U_0. \quad (28)$$

It can be seen that the form of U_s is consistent with Eq. (18) in [12]. To find U_0 we need to calculate out

$$f_{0,2} - f_{0,4} + f_{0,6} - f_{0,7} + f_{0,9} - f_{0,8}. \quad (29)$$

Applying the MBB rule

$$f_{0,7} = f_{0,9} \quad f_{0,6} = f_{0,8} \quad f_{0,3} = f_{0,5}, \quad (30)$$

we only need to consider $f_{0,2} - f_{0,4}$. After simple calculations using Eqs. (25b) and (25d) (note that the MBB rule allows collisions at boundary, and again, these two equations are actually determined by the periodic boundary condition) with the prescribed boundary velocity ($u_0 = 0, 0$), we find it equals

$$f_{0,2} - f_{0,4} = \frac{2}{3} g_x \rho \tau. \quad (31)$$

Regarding that

$$g_x = \frac{8\mu u_m}{L^2 \rho}, \quad (32)$$

where u_m denotes the centerline speed without slip velocity at boundaries, U_s is written as

$$U_s = -g_x(dt_9 - 2\tau) = -\frac{8\mu(dt_9 - 2\tau)u_m}{L^2 \rho}, \quad (33)$$

which is in the form of physical dimension. To transform to the commonly used lattice unit, we uses relations

$$\mu = \rho R T_0 \tau \quad L = N dx = N dt_9 \sqrt{3RT_0} \quad (34)$$

and

$$\hat{\tau} = \frac{\tau}{dt_9} + \frac{1}{2}, \quad (35)$$

which yields

$$U_s = \frac{8(\hat{\tau} - 1)(2\hat{\tau} - 1)u_m}{3N^2}. \quad (36)$$

Here the units of U_s and u_m is not important since they cancel each other. We note the form Eq. (36) is slightly different from Eq. (22) in [12]. This is mainly because of difference of the factor B , i.e., the treatment of the body force term, cf. Eq. (4) and Eq. (1) in [12].

Clearly, the non-physical slip velocity obtained in [12] is due to the contribution of $f_{0,2}$ and $f_{0,4}$. However, as we have stressed, they are mainly the consequence of periodic boundaries at the streamwise direction. Therefore, the failure of the MBB scheme is due to lack of definition on the behaviour of discrete velocities parallel to wall. Then, they are actually controlled by other factors. In this case, it is the boundary scheme used in the inlet and outlet, which is not the bounce-back scheme.

In this way, the slip velocity may be arbitrary in numerical practice, which may depend on the specific inlet and outlet boundary condition, geometry, other numerical operations at the boundary, and even the initial condition at wall.

By identifying the mechanism of non-physical slip velocity, we may be able to devise remedy for the BB scheme. The key is to supplement the definition for the behaviour of the discrete velocities parallel to wall if there are any. Since other distribution function pairs can cancel each other when obtaining the velocity, they must also be able to cancel each other so that the velocity is zero. For instance, in this force-driven Poiseuille flow, although the bulk points must admit the consequence of the inlet and outlet boundary conditions, wall boundary points do not have to do so. In other words, we do not necessarily need to apply rules Eqs. (25b) and (25d) which has been done above and in [12]. By contrary, We may initially set $f_{0,2}$ and $f_{0,4}$ to be a equilibrium distribution with zero velocity and they can remain their initial state all the time. This simple fix is able to correctly yield zero slip velocity.

In practice, this can be incredibly easy for simple geometries. In the following section, we will show that actually no extra effort is necessary for a lid-driven cavity flow. However, the solution for complex geometries may need further investigation.

On the other hand, it is worth noting that extra care may be necessary when using Eq. (36) to analyse the accuracy. At a first glance, U_s seems to be a second order small quantity. However, in Eq.(33), it is actually more or less a constant error since we should set dt_9 to be smaller than τ for stability while both g_x and τ are constant for a given incompressible and isothermal flow configuration. In our view, that is the confusion caused by using numerical time/spatial steps as reference quantities.

C. D2Q9 simulations for lid-driven cavity flow

In this section, we will show how to utilise the above observation to devise remedy for the non-physical slip velocity. For this purpose, we will simulate the lid-driven cavity flow using the D2Q9 model. At the bottom, left and right wall, we will implement the bounce-back scheme. The non-equilibrium bounce-back scheme [18] is adopted for the top moving wall to bring in a wall velocity.

For the cavity flow, we notice a fact that, for the discrete velocities parallel to wall, their distributions at boundary nodes are never affected by those of bulk. For the BB scheme, they will only be affected by their neighbours at wall. For the MBB scheme, the local collisions will also come into play. This fact can be utilised for eliminating the slip velocity.

For the BB scheme, it can be easily seen that, for the discrete velocities parallel to wall (e.g., \mathbf{C}_2 and \mathbf{C}_4 for the bottom wall), the initial state is actually maintained in a way that the information is cycling among wall nodes. If the initial conditions at all wall nodes are set to be the uniform equilibrium distribution with zero velocity, the distribution of such as \mathbf{C}_2 and \mathbf{C}_4 will always be able to cancel each other when finding the velocity. Therefore, the non-slip velocity boundary can be achieved without any extra effort. The corner points at the top wall are a little more tricky as they are singular points. In practice, they may be treated as either a top wall point or a point of the left or right wall. Here, to maintain the benefit of “no extra” effort, we need to treat them as a left or right wall point. Otherwise, distributions at the left and right wall will be affected by those of the top wall which are changing with time, and the initial equilibrium state with zero velocity will break down. The other two corner points can be treated in normal way although more discrete velocities need to be “bounced back”.

For the MBB scheme, as collisions will occur at boundary points, the initial state cannot be maintained. However, using the fact that the information can not propagate into the bulk for the discrete velocities parallel to the wall, we are able to blend the relevant distribution to obtain the nonslip condition at wall. For instance, for the bottom wall, we can use the average of distribution of \mathbf{C}_2 and \mathbf{C}_4 as their new value after the streaming step.

Numerical simulations are conducted for both two ways with four different Reynolds numbers while the top wall speed is fixed as $0.1\sqrt{RT_0}$. To examine the speed at the bottom, left, and right wall, we calculate the sum of $\sqrt{\mathbf{U} \cdot \mathbf{U}}$ of all nodes at these three walls at every

	$Re = 10$	$Re = 100$	$Re = 500$	$Re = 1000$
Average speed (no collision at wall, $\times 10^{-18}$)	8.774	8.740	8.831	8.844
Average speed (with collision at wall, $\times 10^{-18}$)	11.663	11.594	11.596	11.610

Table I. Average speed at the bottom, left, and right wall. The top wall speed is $0.1\sqrt{RT_0}$.

time step and then obtain the average speed per time step and per node. Since we are not examine the solution accuracy, no convergence test will be done for mesh size. By contrary, we will use as coarse mesh as possible to obtain results quickly. The maximum time step is set to be 10,000 iterations. While it is not of interest if the steady state is approached, the first order time derivative of the L^2 norm error of velocity is found to be smaller than 3.5×10^{-4} except for cases with $Re = 1000$. The results are summarised in Table I. As has been shown, the speed at walls are effectively zero within the machine resolution (double precision). It is worth noting again that actually no extra effort is necessary for the BB scheme.

IV. CONCLUDING REMARKS

To conclude, we have investigated the issue of the slip velocity at wall boundaries in lattice Boltzmann simulations with the BB scheme family. To identify the mechanism, we have analytically compared the solutions of a D2Q4 lattice and the commonly used D2Q9 lattice for the force-driven Poiseuille flow. It is found that the BB family scheme does not define the behaviour of discrete velocities parallel to the wall. Mathematically the boundary condition is **incompletely determined**. This gives opportunities for other factors to affect them, such as the boundary conditions for inlet and outlet or even the initial condition at boundary. The non-physical slip velocity are induced exactly by these undesired effects. Therefore, the scheme for the bulk (e.g., the SRT scheme) is not the intrinsic reason for the slip velocity.

To solve this issue, the key is to supplement the definition for the discrete velocities parallel to wall. By simulating the lid-driven cavity flows, We have shown that this can be incredibly easy for simple geometries. In fact, we may need no extra effort . The future study is to find if there is similar solution for complex geometries, which is already under progress.

ACKNOWLEDGMENTS

The authors would like to thank the Engineering and Physical Science Research Council (EPSRC) for their support of Collaborative Computational Project 12 and 5. Jianping Meng would like to thank Prof. Chao-an Lin at the National Tsing Hua University for his help on the procedure presented in [12].

- [1] S. Chen and G. D. Doolen, *Annu. Rev. Fluid Mech.* **30**, 329 (1998).
- [2] Y. H. Qian, S. Succi, and S. A. Orszag, *Annu. Rev. Comput. Phys.* **III**, 195 (1995).
- [3] C. K. Aidun and J. R. Clausen, *Ann. Rev. Fluid Mech.* **42**, 439 (2010).
- [4] U. Frisch, B. Hasslacher, and Y. Pomeau, *Phys. Rev. Lett.* **56**, 1505 (1986).
- [5] X. He and L.-S. Luo, *Phys. Rev. E* **55**, R6333 (1997).
- [6] X. He and L.-S. Luo, *Phys. Rev. E* **56**, 6811 (1997).
- [7] X. Shan and X. He, *Phys. Rev. Lett.* **80**, 65 (1998).
- [8] X. W. Shan, X. F. Yuan, and H. D. Chen, *J. Fluid Mech.* **550**, 413 (2006).
- [9] R. Mei and W. Shyy, *J. Comput. Phys.* **143**, 426 (1998).
- [10] H. Xi, G. Peng, and S.-H. Chou, *Phys. Rev. E* **59**, 6202 (1999).
- [11] R. Cornubert, D. d’Humières, and D. Levermore, *Physica D* **47**, 241 (1991).
- [12] X. He, Q. Zou, L.-S. Luo, and M. Dembo, *J. Stat. Phys.* **87**, 115 (1997).
- [13] L.-S. Luo, W. Liao, X. Chen, Y. Peng, and W. Zhang, *Phys. Rev. E* **83**, 056710 (2011).
- [14] C. Pan, L.-S. Luo, and C. T. Miller, *Computers & Fluids* **35**, 898 (2006), proceedings of the First International Conference for Mesoscopic Methods in Engineering and Science.
- [15] X. He, X. Shan, and G. D. Doolen, *Phys. Rev. E* **57**, R13 (1998).
- [16] X. He, S. Chen, and G. D. Doolen, *J. Comput. Phys.* **146**, 282 (1998).
- [17] J. Meng and Y. Zhang, *J. Comput. Phys.* **230**, 835 (2011).
- [18] Q. Zou and X. He, *Phys. Fluids* **9**, 1591 (1997).